

This research result is published in the journal *Advanced Functional Materials*, 2010

## **1. Introduction**

Fabricating photovoltaic devices using solution-processed materials has many potential benefits, particularly for the rapid and economical preparation of flexible, large-area devices. Solution-processing of organic polymers,<sup>[1,2]</sup> inorganic semiconductors,<sup>[3–5]</sup> and organic/inorganic hybrids<sup>[6–9]</sup> has been adopted widely. One example of the use of conjugated polymers is in the preparation of heterojunction photovoltaic devices, which have achieved solar conversion efficiencies greater than 6%.<sup>[10]</sup> Nevertheless, because composites of low-bandgap conjugated polymers and fullerene derivatives remain active only at wavelengths from 300 to 800 nm, they fail to harvest most of the radiation in the infrared (IR) spectral region. By virtue of the quantum size effect, colloidal quantum dots (QDs) of Pb salts have absorption characteristics that can be tuned throughout the IR spectrum.<sup>[11–13]</sup> Furthermore, colloidal Pb-salt QDs can potentially undergo multiple exciton generation,<sup>[14,15]</sup> the generation of more than one electron/hole pair. If multiexciton formation, dissociation, and charge collection were all efficient events, the resulting enhanced photocurrent would lead to an increase in the solar energy conversion efficiency.<sup>[16]</sup> Hence, the development of Pb-salt colloidal QDs for use in optoelectronic devices has emerged recently as an active area of investigation.<sup>[17–20]</sup>

Using a layer-by-layer (LBL) technique—one that involves alternate (i) dip-coating or spin-coating of QDs onto a patterned indium tin oxide (ITO) substrate and (ii) exposing the QD films to a bidentate ligand to can effectively remove the long, insulating oleate ligands from the as-synthesized PbSe QDs—has resulted in increased conductivities of PbSe QD films and excellent photovoltaic performance.<sup>[4,5,21]</sup> The first example of the use of LBL processing of PbSe QDs to form a double-layer device structure led to an AM1.5 power conversion efficiency (PCE) of 1.1%.<sup>[22]</sup> Later, it was demonstrated that PbSe QD photovoltaic devices exhibit superior performance, with AM1.5 PCEs of ca. 2.1%.<sup>[23]</sup> Subsequently, large improvements in the open-circuit voltages ( $V_{oc}$ ) were obtained when combining  $PbS_xSe_{1-x}$  QDs<sup>[24]</sup> or PbSe QD/ZnO heterojunctions<sup>[25,26]</sup> with the LBL technique, resulting in higher PCEs.

Because a completed QD active layer can feature more than 20 layers processed individually using the LBL technique, the quality of the interfaces between these layers is critical for good charge transport to occur across them and to achieve good device performance.<sup>[27]</sup> Moreover, the alignment between the valence band of the QDs and the work function of the metal oxide anode will affect the open-circuit voltage of the photovoltaic devices. Hence, a high-quality interface must exist between the anode of the device and the first QD layer. In this study, we introduced a thin (ca. 20 nm) poly(3,4-ethylenedioxythiophene): poly(styrene sulfonate) (PEDOT:PSS) hole transport layer into the interface between a tri-layered PbSe QD active layer

Report Documentation Page				Form Approved OMB No. 0704-0188	
Public reporting burden for the collection of information is estimated to average 1 hour per response, including the time for reviewing instructions, searching existing data sources, gathering and maintaining the data needed, and completing and reviewing the collection of information. Send comments regarding this burden estimate or any other aspect of this collection of information, including suggestions for reducing this burden, to Washington Headquarters Services, Directorate for Information Operations and Reports, 1215 Jefferson Davis Highway, Suite 1204, Arlington VA 22202-4302. Respondents should be aware that notwithstanding any other provision of law, no person shall be subject to a penalty for failing to comply with a collection of information if it does not display a currently valid OMB control number.					
1. REPORT DATE <b>25 AUG 2010</b>		2. REPORT TYPE <b>Final</b>		3. DATES COVERED <b>10-02-2009 to 21-08-2010</b>	
4. TITLE AND SUBTITLE <b>High-Sensitivity Conjugated Polymer/Nanoparticle Nanocomposites for Infrared Sensor Applications III</b>				5a. CONTRACT NUMBER <b>FA23860914039</b>	
				5b. GRANT NUMBER	
				5c. PROGRAM ELEMENT NUMBER	
6. AUTHOR(S) <b>Kung-Hwa Wei</b>				5d. PROJECT NUMBER	
				5e. TASK NUMBER	
				5f. WORK UNIT NUMBER	
7. PERFORMING ORGANIZATION NAME(S) AND ADDRESS(ES) <b>National Chiao Tung University,1001 Ta Hsueh Rd,Hsinchu, Taiwan,TW,30049</b>				8. PERFORMING ORGANIZATION REPORT NUMBER <b>N/A</b>	
9. SPONSORING/MONITORING AGENCY NAME(S) AND ADDRESS(ES) <b>Asian Office of Aerospace Research &amp; Development, (AOARD), Unit 45002, APO, AP, 96338-5002</b>				10. SPONSOR/MONITOR'S ACRONYM(S) <b>AOARD</b>	
				11. SPONSOR/MONITOR'S REPORT NUMBER(S) <b>AOARD-094039</b>	
12. DISTRIBUTION/AVAILABILITY STATEMENT <b>Approved for public release; distribution unlimited</b>					
13. SUPPLEMENTARY NOTES					
14. ABSTRACT <b>We prepared photovoltaic devices featuring a PEDOT:PSS hole transport layer and three individually deposited PbSe QD layers. The PbSe photovoltaic devices incorporating the PEDOT:PSS layer exhibited enhanced AM1.5 PCEs relative to those of devices lacking the hole transport layer, with an enhancement factor of 60%. The roughness of the interface between the PEDOT:PSS and PbSe QD layers was almost three times less than that of the original ITO/PbSe QD interface, as measured using X-ray reflectivity. Hence, the presence of the PEDOT:PSS layer not only provided a smoother interface between the PbSe QD layers and the ITO substrate but also resulted in enhanced open-circuit voltages. In addition, the presence of the PEDOT:PSS hole transport layer prolonged the life time, as measured in terms of the time required to reach 80% of the normalized efficiency, of the PbSe QD solar device by six-fold, suggesting that this approach improves the performance of PbSe QD photovoltaic devices.</b>					
15. SUBJECT TERMS <b>Nanocomposites, Polymer composites, Infrared Technology</b>					
16. SECURITY CLASSIFICATION OF:			17. LIMITATION OF ABSTRACT <b>Same as Report (SAR)</b>	18. NUMBER OF PAGES <b>13</b>	19a. NAME OF RESPONSIBLE PERSON
a. REPORT <b>unclassified</b>	b. ABSTRACT <b>unclassified</b>	c. THIS PAGE <b>unclassified</b>			

and ITO substrate to improve the interfacial smoothness and band alignment and, thereby, enhance the device's photovoltaic performance and life time. The fabrication of these devices is described in the Experimental section; the device structure comprised an ITO anode, Al/Ca cathode, and PbSe QD active layer, with or without a PEDOT:PSS layer.

## 2. Results and Discussion

**Figure 1** displays the current density–voltage characteristics of a device incorporating a 95-nm-thick layer of 4.5-nm-diameter PbSe QDs under AM 1.5G conditions ( $100 \text{ mW cm}^{-2}$ ,  $25^\circ\text{C}$ ) and in the dark. The dark current curves of the devices reveal a turn-on voltage of ca. 0.1 V. The PCE for the device incorporating a 20-nm-thick PEDOT:PSS layer was 2.4%, up from 1.5% for the standard device. This increase of 60% in the PCE of the device incorporating the PEDOT:PSS layer, relative to that of the standard device, resulted from increases in the values of both  $V_{oc}$  and the short-circuit current density ( $J_{sc}$ ). The value of  $V_{oc}$  of 0.24 V for the device featuring the PEDOT:PSS layer was ca. 33% greater than that of 0.18 V for the standard device. The increase in  $V_{oc}$  can be explained in terms of the superior interfacial energy level offset in the device in the presence of the PEDOT:PSS layer than in its absence. Because the incorporated PEDOT:PSS layer has a work function of 5.1 eV, positioned between the valence band of 5.3 eV  $eV^{[25,28]}$  for the 4.5-nm-diameter PbSe QDs and the work function of 4.8 eV of the ITO electrode, this kind of band energy alignment facilitates the transport of dissociated holes to the anode.

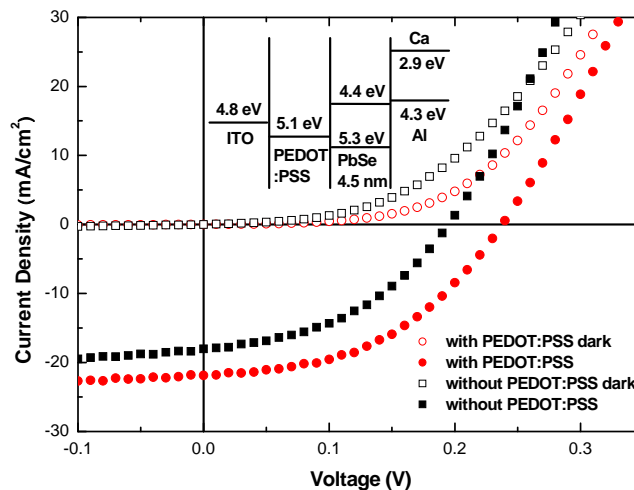


**Figure 1.** Current density–voltage characteristics of 4.5-nm-diameter PbSe QD devices incorporating a PEDOT:PSS intermediate layer, recorded in the dark and under solar illumination ( $100 \text{ mW cm}^{-2}$ ). Inset: Energy-level diagram for a PbSe QD photovoltaic device.

The inset of **Figure 1** displays the energy band diagram for the various layers in the device. The value of  $J_{sc}$  increased to  $21.9 \text{ mA cm}^{-2}$  for the device incorporating the PEDOT:PSS layer

from  $18.0 \text{ mA cm}^{-2}$  for the unmodified device, an increase of ca. 20%, presumably because of superior interfacial contacts and, therefore, improved carrier transport between the PbSe QDs and the PEDOT:PSS layer. The fill factors (FFs) of these two devices, however, were similar. **Table 1** lists the current density–voltage characteristics of the PbSe QD device, incorporating a PEDOT:PSS intermediate layer, under  $100 \text{ mW cm}^{-2}$  solar AM1.5G illumination.

**Table 1.** Performance parameters of PbSe QD devices incorporating a PEDOT:PSS intermediate layer, under solar illumination.

Device structure	$V_{oc}^a$ (V)	$J_{sc}^b$ ( $\text{mA cm}^{-2}$ )	FF <sup>c</sup> (%)	$\eta^d$ (%)
ITO/PbSe/Ca/Al	0.19	18.0	44.0	1.5
ITO/PEDOT:PSS/PbSe/Ca/Al	0.24	21.9	45.5	2.4

<sup>a</sup>  $V_{oc}$ : Open-circuit voltage. <sup>b</sup>  $J_{sc}$ : Short-circuit current density. <sup>c</sup> FF: Fill factor. <sup>d</sup>  $\eta$ : PCE. Solar: AM1.5G ( $100 \text{ mW cm}^{-2}$ ).

**Figure 2a** presents a cross-sectional TEM image of a device incorporating a PEDOT:PSS layer (thickness: 20 nm) and a PbSe QD active layer (thickness:  $95 \pm 5 \text{ nm}$ ); two interfaces are clearly evident in the active layer (i.e., PbSe-1–PbSe-2 and PbSe-2–PbSe-3). The thickness of this active layer (ca. 95 nm) is close to the optimal value for PbSe QDs devices.<sup>[23–25]</sup> Closer examination on the TEM image of the ITO/PEDOT:PSS/PbSe QDs/Ca/Al device structure revealed that the PbSe QDs formed a dense layer that was in intimate physical contact with the PEDOT:PSS layer. The PEDOT:PSS layer apparently provided a smooth transition from the rough ITO surface to the PbSe QD layer. The formation of a smooth active layer, an important feature for efficient device operation, presumably resulted from strong polar interactions between the PbSe QDs and the PEDOT:PSS layer.<sup>[29]</sup> Furthermore, the interfacial roughness among the PbSe QD layer, the incorporated PEDOT:PSS layer, and the ITO substrate could be determined quantitatively using synchrotron X-ray reflectivity (XRR) measurements. **Figure 2b** presents XRR curves of the PbSe QD films on ITO substrates, in the presence and absence of the PEDOT:PSS layer. The curve of the device incorporating the PEDOT:PSS layer exhibits oscillating behavior between  $0.3$  and  $1.0 \text{ nm}^{-1}$ ; that of the device lacking a PEDOT:PSS layer appears to be much smoother, providing further evidence that the PEDOT:PSS layer reduced the interfacial roughness of this device.

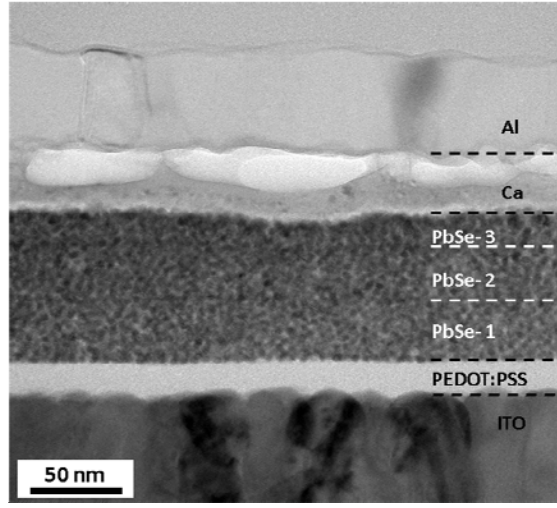


**Figure 2.** (a) TEM cross-sectional image of the ITO/PEDOT:PSS/PbSe QD film/Ca/Al device stack; scale bar: 50 nm.

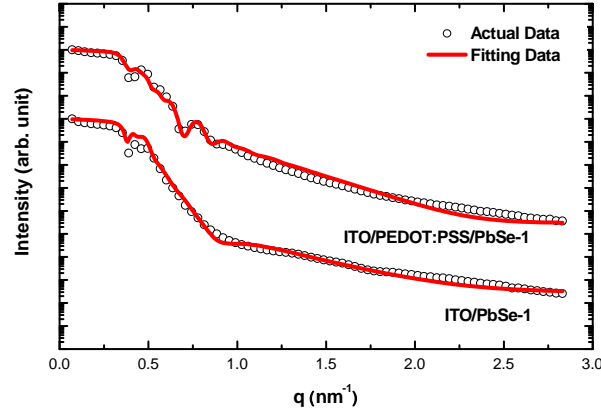


**Figure 2.** (b) Synchrotron X-ray reflectance for structures incorporating PbSe QD layers, prepared with and without a PEDOT:PSS thin layer.

**Table 2** lists the interfacial roughness parameters obtained from curve-fitting the XRR data.<sup>[30]</sup> The device prepared without a PEDOT:PSS layer between the ITO substrate and the PbSe layer had a roughness,  $\sigma_{\text{ITO/PbSe-1}}$ , of 2.9 nm. After incorporating a PEDOT:PSS layer on the ITO substrate, the roughness of the interface between the PEDOT:PSS and PbSe QD layers,  $\sigma_{\text{PEDOT:PSS/PbSe-1}}$ , became 1.0 nm, almost a three-fold improvement with respect to that of the original ITO–PbSe QD interface. Furthermore, the fitting results revealed that the PEDOT:PSS layer not only reduced the interfacial roughness of the ITO/PbSe QD substrate but also smoothed the interface between the individually spun PbSe QD layers; the value of  $\sigma_{\text{PbSe-1/PbSe-2}}$  decreased to 2.8 nm in the presence of PEDOT:PSS layer, from 5.0 nm in its absence.

**Table 2.** Interfacial roughness data obtained by fitting the XRR curves of various layer structures.

ITO/PbSe QDs structure interfacial roughness	nm	ITO/PEDOT:PSS/PbSe QDs structure interfacial roughness	nm
$\sigma_{\text{ITO/PbSe-1}}$	2.9	$\sigma_{\text{ITO/PEDOT:PSS}}$	3.1
—	—	$\sigma_{\text{PEDOT:PSS/PbSe-1}}$	1.0
$\sigma_{\text{PbSe-1/PbSe-2}}$	5.0	$\sigma_{\text{PbSe-1/PbSe-2}}$	2.8

**Figure 3a** presents current density–voltage plots of PbSe QDs devices featuring various QD sizes in the presence of the PEDOT:PSS layer; **Table 3** lists the photovoltaic properties of these PbSe QD devices. The value of  $V_{oc}$  of the device decreases from 0.24 to 0.14 V, while the value of  $J_{sc}$  decreased from 21.9 to 17.7  $\text{mA cm}^{-2}$ , upon increasing the size of the PbSe QDs from 4.5 to 6.0 nm. The decrease in  $V_{oc}$  upon increasing the QD size was due mainly to the corresponding rising of the valence band and the narrowing of the band gap of the PbSe QDs.

**Table 3.** Performance parameters of devices featuring PbSe QDs of various average diameters and incorporating a PEDOT:PSS intermediate layer, under solar illumination.

PbSe QD size (nm)	$V_{oc}$ (V)	$J_{sc}$ ( $\text{mA cm}^{-2}$ )	FF (%)	$\eta$ (%)
6.0	0.14	17.7	34.9	0.86
5.5	0.17	17.8	39.0	1.18
5.2	0.20	18.5	38.2	1.41
4.8	0.23	19.7	43.4	1.97
4.5	0.24	21.9	45.5	2.40

**Figure 3b** presents the values of  $V_{oc}$  of the devices incorporating different sizes of PbSe QDs plotted with respect to their band gaps ( $E_g$ ), which we estimated from their sizes as reported in the literature.<sup>[25,28]</sup> We observe linear behavior in the plots of  $V_{oc}$  against  $E_g$  for the devices containing and lacking the PEDOT:PSS layer. For the devices incorporating a PEDOT:PSS layer, the approximately linear behavior between the values of  $V_{oc}$  and  $E_g$  of the PbSe QDs can be described using the empirical equation

$$V_{oc} = 0.65(E_g / e) - 0.30V \quad (1)$$

where  $e$  is the charge of an electron. The slope (0.65) of the line is close to the value reported in the literature for devices containing similar QDs.<sup>[26]</sup> The decrease in  $J_{sc}$  of the device was caused presumably by increased interfacial roughness when the size of the PbSe QDs increased.

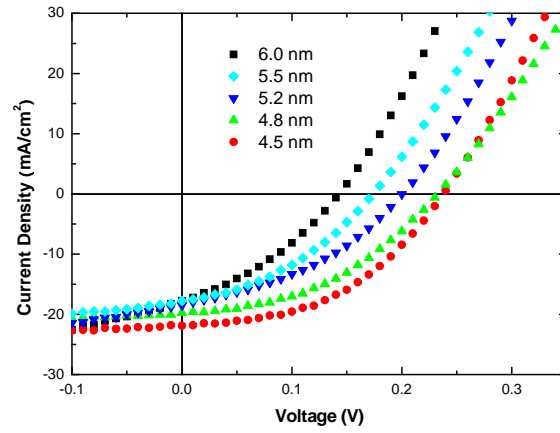


**Figure 3.** (a) Current density–voltage plots of devices incorporating a PEDOT:PSS layer and PbSe QDs of various average diameters.

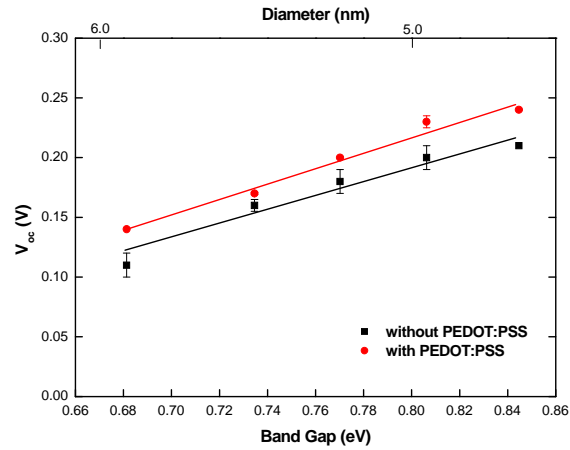


**Figure 3.** (b) Open-circuit voltages ( $V_{oc}$ ) plotted with respect to the diameter of the PbSe QDs and the band gap energy ( $E_g$ ) of the devices prepared with and without a PEDOT:PSS layer.

**Figure 4** presents external quantum efficiency (EQE) curves for the ITO/PbSe QDs/Ca/Al (standard) and ITO/PEDOT:PSS/PbSe QDs/Ca/Al devices in the wavelength region from 300 to 1800 nm. The device incorporating PEDOT:PSS exhibits a larger EQE than that of the standard device from 360 to 1000 nm, covering the entire visible light range and a small portion of near-IR range. At 650 nm, for instance, the EQE reached 57% for the device containing the PEDOT:PSS layer, compared with 46% for the standard device. The theoretical short-circuit current densities obtained after integrating the EQE curves for the device incorporating PEDOT:PSS and for the standard device were 21.6 and 17.9 mA cm<sup>-2</sup>, respectively; these values are close to those (21.9 and 18.0 mA cm<sup>-2</sup>, respectively) obtained directly from the  $I$ – $V$  curves, confirming the accuracy of our measurements. **Figure 5** reveals that an approximately linear

relationship exists between the short-circuit current density and the incident light intensity over the range from 0 to  $100 \text{ mW cm}^{-2}$ , suggesting that this type of device might also find use as a photodetector.

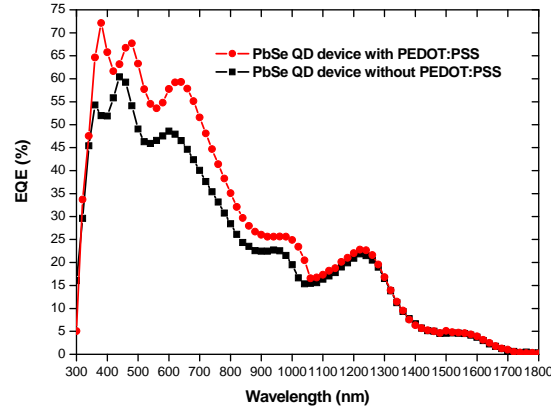


**Figure 4.** EQE spectra of PbSe QD devices prepared with and without a PEDOT:PSS layer.

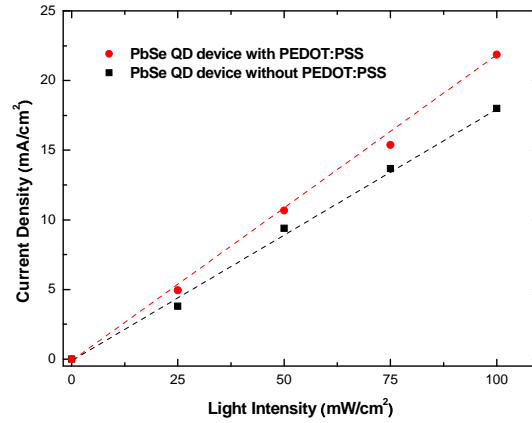


**Figure 5.** Photocurrent density ( $J_{sc}$ ) plotted with respect to the intensity of solar light for the PbSe QD device prepared with and without a PEDOT:PSS layer.

Next, we tested the durability of our solar device under simultaneous and continuous AM1.5G illumination and current–voltage scanning. Because PbSe QD–based devices are air-sensitive, with instantaneous degradation having been reported upon their exposure to air,<sup>[19,23]</sup> all of our devices were packaged before being measured under ambient conditions. **Figure 6** reveals that the stability of the PCE of the device incorporating the PEDOT:PSS layer was substantially greater relative to that of the device lacking the PEDOT:PSS layer. In particular, the device life times, measured in terms of the time required to reach 80% of the normalized efficiency, for the standard PbSe QD device and the PbSe QD device incorporating the



PEDOT:PSS layer were 20 and 120 min, respectively, a six-fold improvement for the latter. Notably, the device incorporating the PEDOT:PSS layer exhibited almost constant values of  $J_{sc}$  and FF during its first 60 min of operation; in contrast, its value of  $V_{oc}$  decreased gradually.

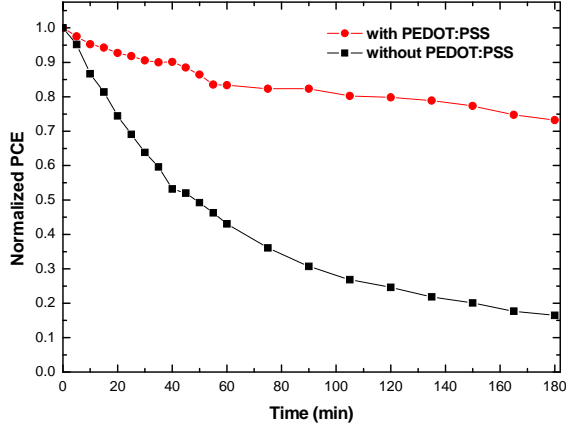


**Figure 6a.**

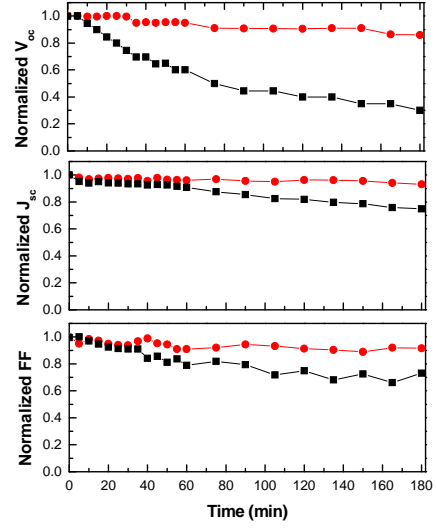


**Figure 6b.**

**Figure 6.** Values of (a) PCE, (b)  $V_{oc}$ ,  $J_{sc}$ , and FF, measured as a function of time and normalized with respect to their initially measured values, for devices prepared with and without a PEDOT:PSS intermediate layer, illuminated continuously under simulated AM1.5G irradiation ( $100 \text{ mW cm}^{-2}$ ).

### 3. Conclusions

We have prepared photovoltaic devices featuring a PEDOT:PSS hole transport layer and three individually deposited PbSe QD layers. The PbSe photovoltaic devices incorporating the PEDOT:PSS layer exhibited enhanced AM1.5 PCEs relative to those of devices lacking the hole transport layer, with an enhancement factor of 60%. The roughness of the interface between the PEDOT:PSS and PbSe QD layers was almost three times less than that of the original ITO–PbSe QD interface, as measured using X-ray reflectivity. Hence, the presence of the PEDOT:PSS layer not only provided a smoother interface between the PbSe QD layers and the ITO substrate but also resulted in enhanced open-circuit voltages. In addition, the presence of the PEDOT:PSS hole transport layer prolonged the life time, as measured in terms of the time required to reach 80% of the normalized efficiency, of the PbSe QD solar device by six-fold, suggesting that this approach improves the performance of PbSe QD photovoltaic devices.

## 4. Experimental

**Materials:** Lead(II) oxide (PbO, 99.99%) was obtained from Alfa Aesar. Selenium (Se, 99.9%), oleic acid (OA, tech. 90%), trioctylphosphine (TOP, tech. 90%), 1-octadecene (ODE, tech. 90%), butylamine (BA, 99.5%), and 1,2-ethanedithiol (EDT, 98%) were purchased from Sigma–Aldrich. Octane (HPLC-grade) and acetonitrile (anhydrous) were obtained from TEDIA. Methanol (anhydrous), toluene (anhydrous), and isopropanol (anhydrous) were obtained from J. T. Baker.

**PbSe QDs:** The QDs were synthesized using standard Schlenk line techniques under an Ar flow; the PbSe used in this study was synthesized according to the method reported by Yu et al [31]. PbO (0.8920 g, 4.000 mmol), oleic acid (2.825 g, 10.00 mmol), and ODE (12.83 g) were stirred together in a three-neck flask and heated at 160 °C under continuous Ar flow for 30 min to obtain a colorless, clear solution. At this temperature, 10% Se-TOP solution (6.4 g) was quickly injected into the solution, dropping the temperature to ca. 150 °C for the growth process. After allowing the reaction to proceed for 30–120 s, the mixture was quenched by placing it in a water/ice bath for 1 min. The colloidal QDs were isolated from the growth mixture through repeated precipitations with methanol prior to being dispersed in toluene, vacuum-dried, and stored in a glove box. **Figure 7** displays TEM images of the synthesized PbSe QDs.

**BA Ligand Exchange:** The ligand exchange process was performed in a N<sub>2</sub>-filled glove box, following the method reported by Konstantatos et al [32]. The as-synthesized PbSe colloidal QDs were redispersed (to 50 mg mL<sup>-1</sup>) in anhydrous BA and stirred continuously for 3 days. The resultant QDs were precipitated with anhydrous isopropanol and redispersed in anhydrous octane (80 mg mL<sup>-1</sup>) for device fabrication. This ligand exchange on the PbSe QDs, albeit completed only partially [17, 33], was designed to obtain better film surface structures than that of PbSe QDs without the ligand exchange after spin-coating; see **Figure 8**.

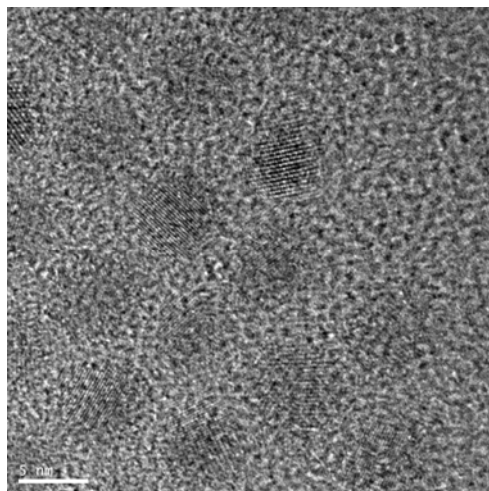


**Figure 7.** High-resolution transmission electron microscopy image of PbSe QDs capped with oleate ligands. Scale bar: 5 nm. The average size of these PbSe QDs was ca.  $5.5 \pm 5$  nm.

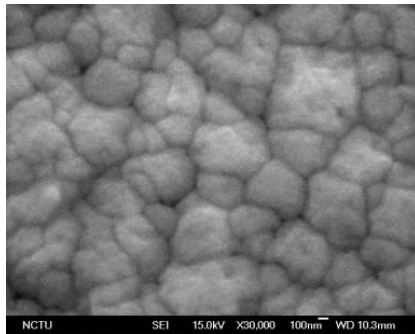


**Figure 8A**

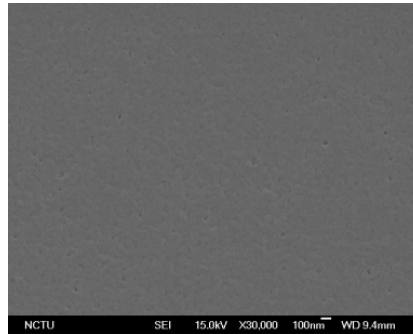


**Figure 8B**

**Figure 8.** Plan-view scanning electron microscopy image of spin-cast PbSe QD films capped with (A) oleate and (B) butylamine ligands.

*Device Fabrication:* The patterned ITO on the glass substrate ( $5 \Omega \text{ sq}^{-1}$ , Merck) was cleaned through sequential ultrasonic treatment (30 min) with 2% detergent, methanol, acetone, and isopropanol and then dried under a flow of  $\text{N}_2$ . PEDOT:PSS (Baytron P VP AI 4083) was then spin-coated on the ultraviolet ozone-treated ITO. After annealing the PEDOT:PSS film at  $150^\circ\text{C}$  for 10 min, the PbSe QDs in anhydrous octane were spin-coated onto the PEDOT:PSS layer on the patterned ITO; the samples were then soaked in 0.01 M EDT in anhydrous acetonitrile for several seconds to enhance the film conductivity. The fabrication of the photovoltaic devices involved several steps: (1) the BA-treated PbSe QDs in octane were spin-coated on the PEDOT:PSS layer that had previously been deposited and dried on the ITO electrode; (2) the whole sample, with its surface PbSe QD layer, was treated with 0.01M EDT; (3) the whole sample was rinsed with anhydrous acetonitrile and octane to remove residual free-standing EDT molecules; (4) the treated sample was dried under a stream of  $\text{N}_2$ . The resulting PbSe QDs layer is referred herein as PbSe-1. A second layer of EDT-treated PbSe QDs (PbSe-2) was prepared on top of the first by repeating this process. Finally, a third layer of PbSe QDs (PbSe-3) was deposited; together, these three individually spun PbSe QD layers served as the active layer. **Figure 9** presents the Fourier transform IR spectrum of the spin-coated PbSe QD films on the ITO substrates before and after treatment with EDT. The sharp decreases in the intensities of the C–H and  $\text{COO}^-$  signals after EDT treatment indicated that most of the oleate ligands on the PbSe QDs had been removed, because thiol–Pb bonds are much stronger than amine–Pb bonds [4]. The thickness of the PbSe QD layer was measured using a Dektak profilometer. Finally, 20-nm Ca and 100-nm Al top electrodes were deposited onto all of the samples at ca.  $10^{-7}$  torr by thermal evaporation through a shadow mask. Four devices were fabricated on each substrate, each with an active area of  $0.04 \text{ cm}^2$ .

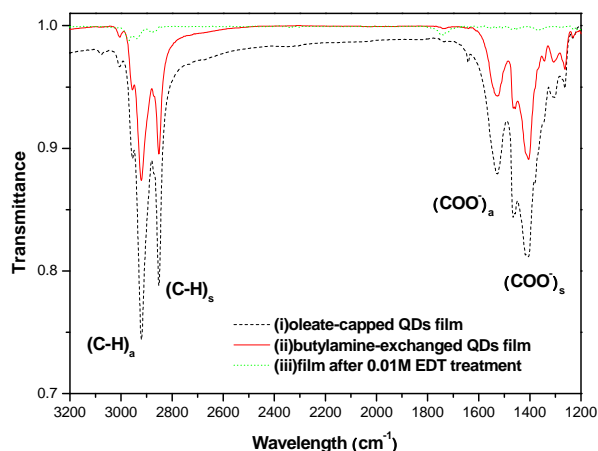


**Figure 9.** Fourier transform infrared spectra of PbSe QD films: (i) oleate-capped, (ii) butylamine-exchanged, and (iii) butylamine-exchanged with subsequent 0.01 M EDT treatment.

*Characterization:* Current density–voltage characteristics of the PbSe QD devices were measured under simulated AM1.5G irradiation ( $100 \text{ mW cm}^{-2}$ ) using a Xe lamp–based Newport 66902 150-W solar simulator equipped with a Keithley 236 source measurement unit. The sweeps were performed between +1 and –1 V, with a step size of 0.01 V. For solar cell measurements, the spectrum of the solar simulator was calibrated as follows: A PV-measurement (PVM-154) mono-Si solar cell (NREL calibrated) and a Si photo diode (Hamamatsu S1133) were used to check the irradiation of the exposed area ( $100 \text{ mW cm}^{-2}$ ). The mismatch factor ( $M = 1.34$ ) was obtained by using the PVM-154 cell as the reference cell and the fabricated devices as test cells and recording spectra from 300 to 900 nm at intervals of 10 nm. The PVM-154 cell was combined with a KG-5 filter (350–700 nm passed, Newport) to simulate a reference solar cell having spectral responsivity from 350 to 700 nm. The calibration was based on the IEC-69094-1 spectrum. EQE data were recorded with respect to the Optosolar SPF50 spectrum response. A Si reference cell was used to calibrate the wavelengths of light from 300 to 1060 nm, and a Ge reference cell from 1060 to 1800 nm. Fourier transform infrared (FTIR) spectra were recorded at room temperature using a Perkin–Elmer Spectrum100 instrument. Scanning electron microscopy (SEM) images was acquired using a JEOL JSM-6500F FESEM apparatus operated at accelerating voltages ranging from 5.0 to 15 kV. Transmission electron microscopy (TEM) images were recorded using an FEI Tecnai G<sup>2</sup> instrument operated at 200 keV. Synchrotron X-ray reflectivity (XRR) analyses were performed at the wiggler beamline BL-17B1 using an eight-circle diffractometer at the National Synchrotron Radiation Research Center (NSRRC), Hsinchu, Taiwan; the photon energy was 8 keV and the flux was estimated to be  $10^{11} \text{ photons s}^{-1}$ . The use of two pairs of slits between the sample and the detector provided a typical wave-vector resolution of ca.  $0.001 \text{ nm}^{-1}$  in the vertical scattering plane.

- [1] J. Y. Kim, K. Lee, N. E. Coates, D. Moses, T. Q. Nguyen, M. Dante, A. J. Heeger, *Science* 2007, 317, 222–225.
- [2] a) L. M. Chen, Z. Hong, G. Li, Y. Yang, *Adv. Mater.* 2009, 21, 1434–1449. b) Y. T. Chang, S. L. Hsu, M. H. Su, K. H. Wei, *Adv. Mater.* 2009, 21, 2093–2097.
- [3] I. Gur, N. A. Fromer, M. L. Geier, A. P. Alivisatos, *Science* 2005, 310, 462–465.
- [4] J. Tang, X. Wang, L. Brzozowski, D. A. R. Barkhosue, R. Debnath, L. Levina, E. H. Sargent, *Adv. Mater.* 2010, 22, 1–5.
- [5] D. V. Talapin, C. B. Murray, *Science* 2005, 310, 86–89.
- [6] S. A. McDonald, G. Konstantatos, S. Zhang, P. W. Cyr, E. J. D. Klem, L. Levina, E. H. Sargent, *Nat. Mater.* 2005, 4, 138–142.
- [7] N. Cho, K. R. Choudhury, R. B. Thapa, Y. Sahoo, T. Ohulchanskyy, A. N. Cartwright, K. S. Lee, P. N. Prasad, *Adv. Mater.* 2007, 19, 232–236.
- [8] H. Y. Chen, M. K. F. Lo, G. Yang, H. G. Monbouquette, Y. Yang, *Nature Nanotechnology* 2008, 3, 543–547.
- [9] Z. Tan, T. Zhu, M. Thein, S. Gao, A. Cheng, F. Zhang, C. Zhang, H. Su, J. Wang, R. Henderson, J. Hahm, Y. Yang, J. Xu, *Appl. Phys. Lett.* 2009, 95, 063510.
- [10] a) J. Hou, H. Y. Chen, S. Zhang, R. I. Chen, Y. Yang, Y. Wu, G. Li, *J. Am. Chem. Soc.* 2009, 131, 15586–15587. b) Y. Liang, Z. Xu, J. Xia, S. T. Tsai, Y. Wu, G. Li, C. Ray, L. Yu, *Adv. Mater.* 2010, DOI: 10.1002/adma.200903528.
- [11] M. A. Hines, G. D. Scholes, *Adv. Mater.* 2003, 15, 1844–1849.
- [12] R. Koole, G. Allan, C. Delerue, A. Meijerink, D. Vanmaekelbergh, A. J. Houtepen, *Small* 2008, 4, 127–133.
- [13] K. Roy Choudhury, Y. Sahoo, T. Y. Ohulchanskyy, P. N. Prasad, *Appl. Phys. Lett.* 2005, 87, 073110.
- [14] M. C. Beard, A. G. Midgett, M. Law, O. E. Semonin, R. J. Ellingson, A. J. Nozik, *Nano Lett.* 2009, 9, 836–845.
- [15] V. Sukhovatkin, S. Hinds, L. Brzozowski, E. H. Sargent, *Science* 2009, 324, 1542–1544.
- [16] R. D. Schaller, V. I. Klimov, *Phys. Rev. Lett.* 2004, 92, 186601.
- [17] J. Tang, X. Wang, L. Brzozowski, D. A. R. Barkhouse, R. Debnath, L. Levina, E. H. Sargent, *Adv. Mater.* 2010, 22, 1398–1402.
- [18] H. Lee, H. C. Leventis, S. J. Moon, P. Chen, S. Ito, S. A. Haque, T. Torres, F. Nüesch, T. Geiger, S. M. Zakeeruddin, M. Grätzel, Md. K. Nazeeruddin, *Adv. Funct. Mater.* 2009, 19, 2735–2742.
- [19] T. Rauch, M. Böberl, S. F. Tedde, J. Fürst, M. V. Kovalenko, G. Hesser, U. Lemmer, W. Heiss, O. Hayden, *Nature Photonics* 2009, 3, 332–336.
- [20] M. S. Kang, J. Lee, D. J. Norris, C. D. Frisbie, *Nano Lett.* 2009, 9, 3848–3852.
- [21] J. M. Luther, M. Law, Q. Song, C. L. Perkins, M. C. Beard, A. J. Nozik, *ACS Nano* 2008, 2, 271–280.
- [22] G. I. Koleilat, L. Levina, H. Shukla, S. H. Myrskog, S. Hinds, A. G. Pattantyus-Abraham, E. H. Sargent, *ACS Nano* 2008, 2, 833–840.

- [23] J. M. Luther, M. Law, M. C. Beard, Q. Song, M. O. Reese, R. J. Ellingson, A. J. Nozik, *Nano Lett.* **2008**, 8, 3488–3492.
- [24] W. Ma, J. M. Luther, H. Zheng, Y. Wu, A. P. Alivisatos, *Nano Lett.* **2009**, 9, 1699–1703.
- [25] J. J. Choi, Y. F. Lim, M. B. Santiago-Berrios, M. Oh, B. R. Hyun, L. Sun, A. C. Bartnik, A. Goedhart, G. G. Malliaras, H. D. Abruña, F. W. Wise, T. Hanrath, *Nano Lett.* **2009**, 9, 3749–3755.
- [26] K. S. Leschkies, T. J. Beatty, M. S. Kang, D. J. Norris, E. S. Aydil, *ACS Nano* **2008**, 3, 3638-3648.
- [27] G. Li, V. Shrotriya, J. Huang, Y. Yao, T. Moriarty, K. Emery, Y. Yang, *Nat. Mater.* **2005**, 4, 864-868.
- [28] D. Cui, J. Xu, T. Zhu, G. Paradee, S. Ashok, M. Gerhold, *Appl. Phys. Lett.* **2006**, 88, 183111.
- [29] D. M. N. M. Dissanayake, R. A. Hatton, T. Lutz, R. J. Curry, S. R. P. Silva, *Nanotechnology* **2009**, 20, 245202.
- [30] L. G. Parratt, *Phys. Rev.* **1954**, 95, 359-369.
- [31] W. W. Yu, J. C. Falkner, B. S. Shih, V. L. Colvin, *Chem. Mater.* **2004**, 16, 3318-3322.
- [32] G. Konstantatos, I. Howard, A. Fischer, S. Hoogland, J. Clifford, E. Klem, L. Levina, E. H. Sargent, *Nature* **2006**, 442, 180-183.
- [33] M. V. Kovalenko, D. V. Talapin, M. A. Loi, F. Cordella, G. Hesser, M. I. Bodnarchuk, W. Heiss, *Angew. Chem. Int. Ed.* **2008**, 47, 3029-3033.